Article

The Electronic, Magnetic, Half-Metallic and Mechanical Properties of the Equiatomic Quaternary Heusler Compounds FeRhCrSi and FePdCrSi: A First-Principles Study

Liefeng Feng [1] (ORCID)**, Jiannan Ma** [1]**, Yue Yang** [1]**, Tingting Lin** [2] **and Liying Wang** [1,]*****

[1] Tianjin Key Laboratory of Low Dimensional Materials Physics and Preparing Technology, Faculty of Science, Tianjin University, Tianjin 300350, China; fengfl@tju.edu.cn (L.F.); majiannan@tju.edu.cn (J.M.); 2018210142@tju.edu.cn (Y.Y.)
[2] Institute of Materials Science, Technische Universtät Darmstadt, 64287 Darmstadt, Germany; ttlin1990@126.com
* Correspondence: liying.wang@tju.edu.cn; Tel.: +86-138-2112-8892

check for updates

Featured Application: Two new 1:1:1:1 quaternary Heusler based half-metals have been designed by means of the first-principles method, and their half-metallic properties are quite robust to the hydrostatic strain or tetragonal distortion.

Abstract: By using the first-principles method, the electronic structures and magnetism of equiatomic quaternary Heusler alloys FeRhCrSi and FePdCrSi were calculated. The results show that both FeRhCrSi and FePdCrSi compounds are ferrimagnets. Both compounds are half-metals and their half-metallicity can be maintained in a wide range of variation of the lattice constant under hydrostatic strain and c/a ratio range under tetragonal distortion, implying that they have low sensitivity to external interference. Furthermore, the total magnetic moments are integers, which are typical characteristics of half-metals. The calculated negative formation energy and cohesive energy indicate that these two alloys have good chemical stability. Furthermore, the value of the elastic constants and the various moduli indicate the mechanical stability of these two alloys. Thus, FeRhCrSi and FePdCrSi are likely to be synthesized in the experiment.

1. Introduction

Since the first half-metal (HM) NiMnSb compound was discovered in 1983 [1], the HM materials have attracted more and more scholars and researchers to investigate. The HM material has a very novel electronic structure, showing semiconducting property in on spin channel and metallic property in the other spin channel [2,3]. This special electronic structure results in a perfect 100% spin polarization near the Fermi level, which makes HM a novel spintronic material. Until now, many different structures of materials have been found to be half-metallic, such as Heusler compounds, dilute magnetic semiconductors, and ferromagnetic metallic oxides, etc. [1–8]. Among them, Heusler compounds are of great importance and present many unique physical properties, including the adjustable electronic structure and relative high Curie temperature [9,10], etc.

Heusler compounds, which have a general formula X_2YZ, are a class of intermetallic compounds (also called full-Heusler compounds). In the formula X_2YZ, X and Y atoms are usually transition metals, and Z is a main group element [11]. For full-Heusler compounds, there are two possible,

different atomic arrangement fashions: the Cu_2MnAl-type and Hg_2CuTi-type structure [12]. Specially, when X and Y are the same atoms, the $D0_3$ structure is formed [13,14]. And when one of the X atoms is substituted with a vacant, the $C1_b$ structure is formed [15]. When one of the X atoms is substituted by another different transition mental, the equiatomic quaternary Heusler compounds (EQHs) (LiMgPdSn structure) with the chemical formula of XMYZ are formed. Recently, several series of EQHs have been found and attracted wide attention. Compared with the binary and ternary Heusler HMs that have been mentioned above, the biggest advantage of the EQH HMs is their lower dissipation, which is caused by their lesser amount of atomic arrangement disorder in experiment [16].

Felser et al. have predicted several EQHs to be theoretical HM ferromagnets and have synthesized them experimentally, such as CoFeMnZ (Z = Al, Si, Ga, Ge), NiFeMnGa and NiCoMnGa [17–20]. Alijani et al. have showed that NiFeMnGa and NiCoMnGa alloys are HM ferromagnets [14]. Gao et al. Reported that CoFeCrAl and CoFeCrSi compounds are several excellent HM ferromagnets [21]. Karimain et al. found that the NiFeTiP and NiFeTiSi alloys are true HM ferromagnets and that the NiFeTiGe has a near HM character [22]. All the above mentioned EQHs are those with 3d transition elements. Very recently, a series of new EQHs with a 4d transition element have been reported. Some of them are as follows: Berri et al. have investigated the robust half-metallicity of the ZrCoTiZ (Z = Si, Ge Ga and In) [23]. The half-metallic and mechanic characters of ZrRhHfZ (Z = Al, Ga and In) [24] and FeCrRuSi [25] were investigated by Wang et al. Guo et al. have reported the excellent half-metallic property of ZrFeVZ (Z = Al, Ga and In) [26]. The new reports of EQHs with a 4d transition element expand the research scope of the spintronic materials. Thus, we can conclude that 4d-transition-elements-contained HMs are new potential spintronic materials worth researching.

In our present work, the electronic, magnetic, half-metallic and mechanical properties of two newly designed EQH compounds, FeRhCrSi and FePdCrSi, were investigated by using the first-principles method. We also have discussed the effect of the hydrostatic strain and tetragonal distortion on their half-metallic properties. And the calculated results indicate that their half-metalicity can be kept in a wide lattice constant range and c/a ratio range. Moreover, the chemical stability and the mechanical properties of FeRhCrSi and FePdCrSi have also been studied in details.

2. Materials and Methods

The electronic and magnetic structures were calculated by using CASTEP code, which was based on the density functional theory (DFT) [27–29]. The ultrasoft pseudopotential was used to described the interactions between the valence electrons and the atomic core. The exchange-correlation energy was calculated under the generalized gradient approximation (GGA) [30,31]. For all calculated cases, the cut-off energy of 450 eV was chosen. The k-points mesh was set as $10 \times 10 \times 10$ [32,33]. The convergence tolerance for all the calculations was selected as a difference on total energy within 5×10^{-6} eV/atom.

3. Results

3.1. Total Energy and Structural Stability

For the LiMgPdSn-type EQH compounds FeRhCrSi and FePdCrSi, due to the different atomic arrangements of them, there are three possibly different crystal structures (here, named as type-1, type-2, and type-3), shown in Figure 1a–c. The atom positions in Wychoff coordinates are also shown in Table 1. In order to get the ground state properties of FeRhCrSi and FePdCrSi, the geometry optimization was performed by calculating the total energy of the FeRhCrSi and FePdCrSi compounds at different lattice constants for the three possible crystal structures. The calculated total energy (E_t) as the function of lattice constants (a) for FeRhCrSi and FePdCrSi compounds (E_t-a curves) are shown in Figure 2. It can be clearly seen that both FeRhCrSi and FePdCrSi compounds of type-1 structure have the lowest total energy, which means the type-1 structure is the most stable configuration. Considering the different magnetic states of these compounds, the total energy as a function of

the lattice constants for the type-1 structure FeRhCrSi and FePdCrSi compounds in ferromagnetic (FM), ferrimagnetic (FIM), and nonmagnetic (NM) states has been calculated (as shown in Figure 3. From Figure 3, it can be found that both FeRhCrSi and FePdCrSi compounds in the FIM state show the lowest total energy. Therefore, for both FeRhCrSi and FePdCrSi compounds, the type-1 structure in the FIM state was the most stable state. Thus, we will focus on discussing the physical properties of these compounds with a type-1 structure and FIM state in the following parts of this paper. And the obtained equilibrium lattice constants at their ground states for FeRhCrSi and FePdCrSi are 5.82 Å and 5.87 Å, respectively, and the results have been shown in Table 2. The small difference of the optimized lattice constants between FeRhCrSi and FePdCrSi compounds derive from the close ionic radii between Rh and Pd atoms.
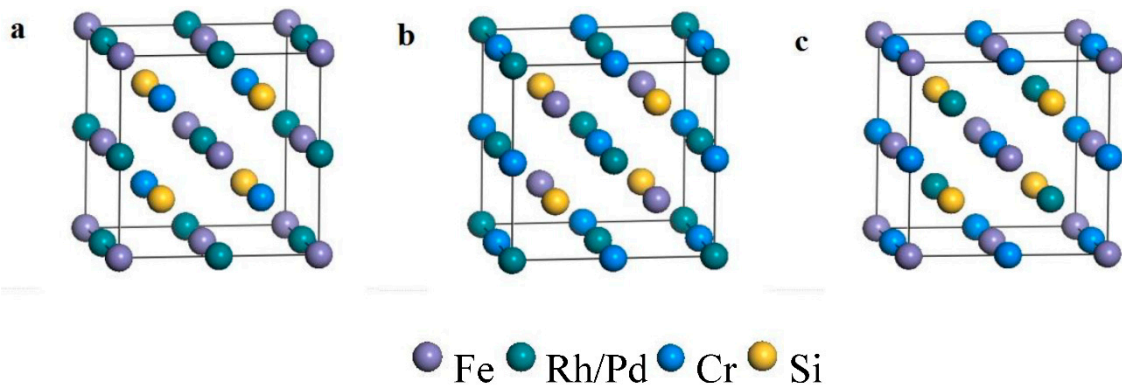

Figure 1. The three possible structures of FeRhCrSi and FePdCrSi (**a**) type-1, (**b**) type-2 and (**c**) type-3.

Table 1. Three possible structures of FeRhCrSi and FePdCrSi.

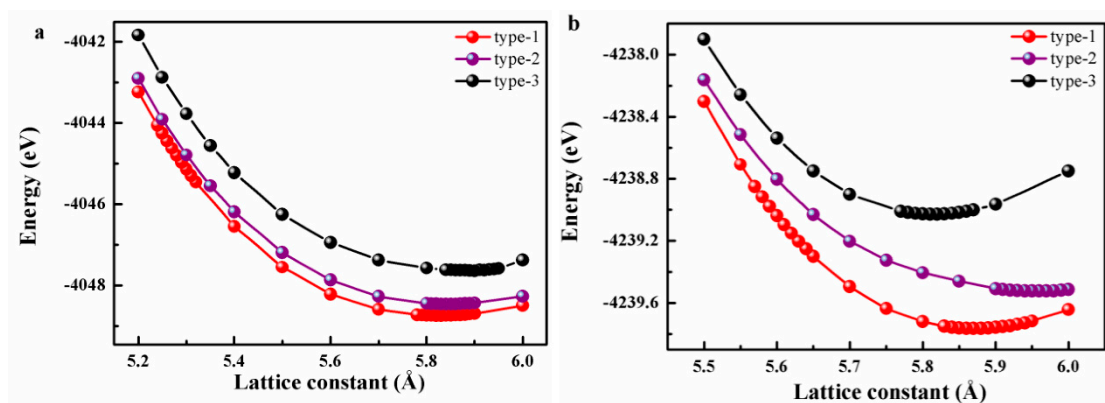| Structure	Fe	Rh/Pd	Cr	Si
Type 1	4a	4c	4b	4d
Type 2	4b	4c	4a	4d
Type 3	4a	4b	4c	4d

Figure 2. Energy optimization with different crystal structures of (**a**) FeRhCrSi and (**b**) FePdCrSi.

Table 2. The optimized equilibrium lattice constant a_0 (Å), the total and partial magnetic moments (μ_B) at the equilibrium lattice, the formation energy E_f and cohesive energy E_c (eV) for the equiatomic quaternary Heusler (EQH) compounds FeRhCrSi and FePdCrSi.

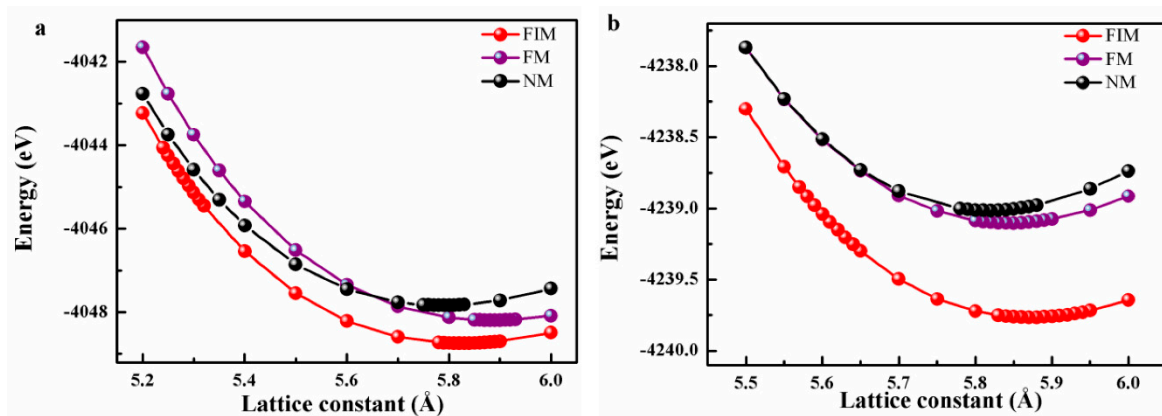| Compounds	a_0	M_{tot}	M_{Fe}	$M_{Rh/Pd}$	M_{Cr}	M_{Si}	E_f	E_c
FeRhCrSi	5.82	3.00	−0.26	0.22	3.10	−0.06	3.12	−20.41
FePdCrSi	5.87	4.00	0.78	−0.14	3.44	−0.08	−1.97	−18.66

Figure 3. Energy optimization with different magnetic states of (**a**) FeRhCrSi and (**b**) FePdCrSi.

3.2. Electronic, Magnetic, and Half-Metallic Properties

In this part, the electronic and magnetic structure of FeRhCrSi and FePdCrSi at their equilibrium lattice constants have been discussed in detail. The calculated band structures of FeRhCrSi and FePdCrSi compounds have been displayed in Figure 4. From Figure 4a,b, it can be found that both FeRhCrSi and FePdCrSi compounds show quite similar band structure characters. In the majority-spin channel, the Fermi level is located in an indirect band gap. The conduction band minimum (CBM) appears at the X point and the valence band maximum (VBM) occurs at the G point of the Brillouin zone. The values of the indirect band gaps in the majority-spin channel are 0.336 eV and 0.177 eV for EQH compounds FeRhCrSi and FePdCrSi, respectively. However, their bands show a metallic cross over at the Fermi level in the minority-spin channel. This results in their 100% spin polarization. Thus, the EQH compounds FeRhCrSi and FePdCrSi are HMs.

Figure 5a,b show the calculated total and partial density of states (DOS) of FeRhCrSi and FePdCrSi at their equilibrium lattice constants. From Figure 5, one can further understand their electronic structures. It can be seen that there is a metallic overlapping with the Fermi level in the minority-spin channel for both the EQH compounds FeRhCrSi and FePdCrSi. By contrast, in the majority-spin direction, the Fermi level locates in a relative wide energy gap (the half-metallic gap). Therefore, the EQH compounds FeRhCrSi and FePdCrSi are HMs that are consistent with the above discussion of their band structures. For FeRhCrSi and FePdCrSi compounds, because of the similar atomic configuration, they present two quite similar total and partial DOS. Here, we take the FeRhCrSi compound as an example and give a detailed discussion on the DOS. From Figure 5a, it can be found that the DOS is mainly dominanted by the Si atom in the lower energy region (−7 eV–5 eV) for the two spin directions. In the energy region −5 eV to −3 eV, the DOS are mainly occupied by Rh-4d states. In the range of −3 eV to −1 eV, except a small contribution of Rh-4d and Cr-3d states, both spin channels are dominated by Fe-3d states. In the energy region around the Fermi level (−1 eV to 1 eV), the energy peak is the result of the common contribution of Fe, Rh, and Cr atoms with d orbitals. It can be observed that, in the minority spin, the main contribution to the DOS is the strong hybridization among the Fe-3d state, Rh-4d state, and Cr-3d state around the Fermi level. In the majority spin, the energy gap mainly comes from the covalent hybridization between the nearest neighbor atoms: Fe and Cr. Galanakis et al. [34] have reported that the formation of the bonding and antibonding states can arise from the strong covalent hybridization between the lower-energy d states (higher-valent) transition metal atom (such as Fe) and the higher-energy d states (lower-valent) transition metal (such as Cr). And then, the half-metallic band gap generates between the bonding and antibonding bands. It has also been reported that, due to the strong intra-atomic exchange interaction, the low valence transition metal atom usually has a large spin splitting [35]. From Figure 5a, it can be found that, compared with Fe and Rh atoms, the Cr atom with a lower valent has a larger spin splitting. Thus, the Cr atom is the main contributor to the total magnetic moment of the FeRhCrSi compound.
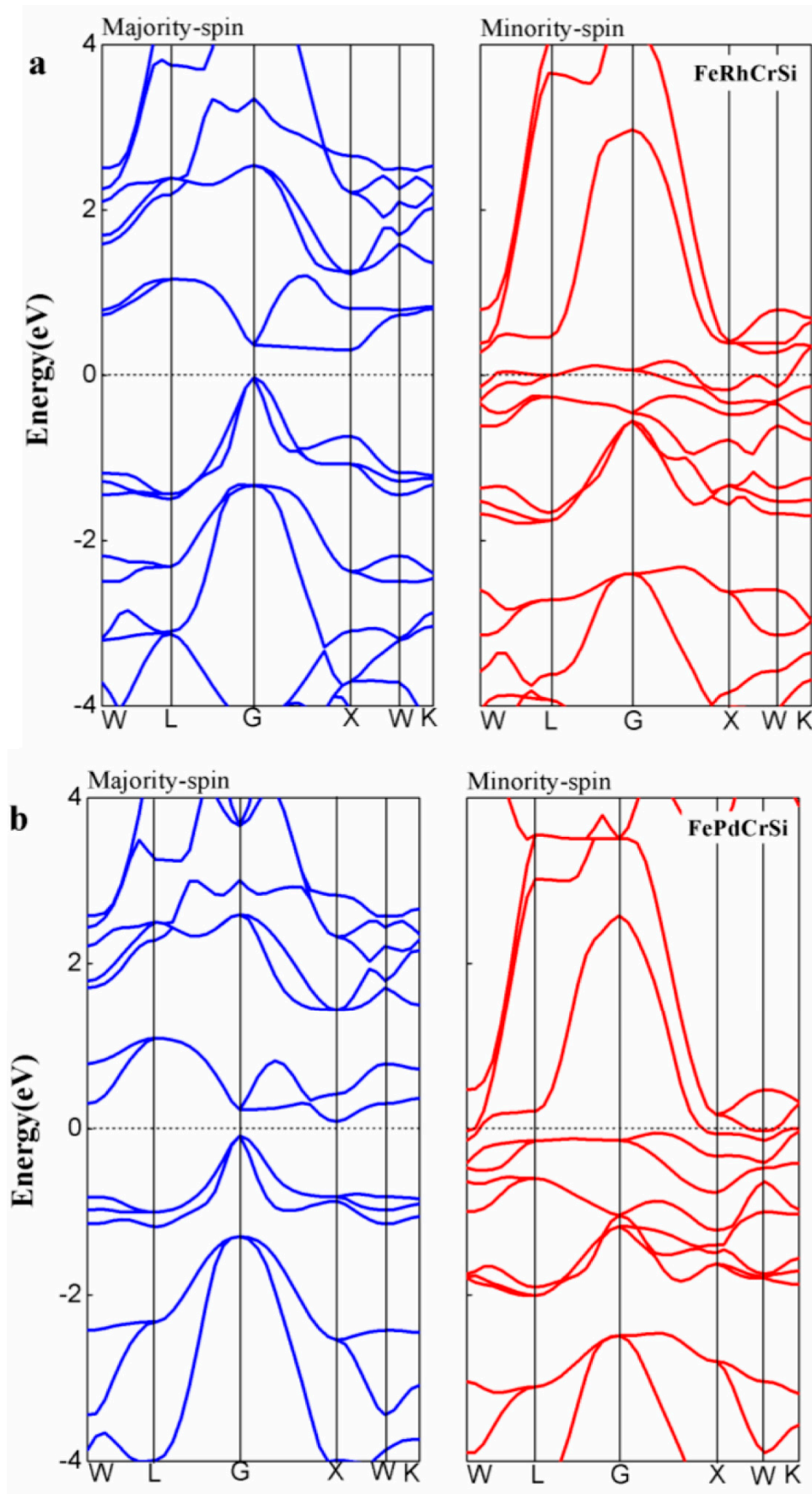
Figure 4. The band structures of (**a**) FeRhCrSi and (**b**) FePdCrSi at their equilibrium lattice constants.
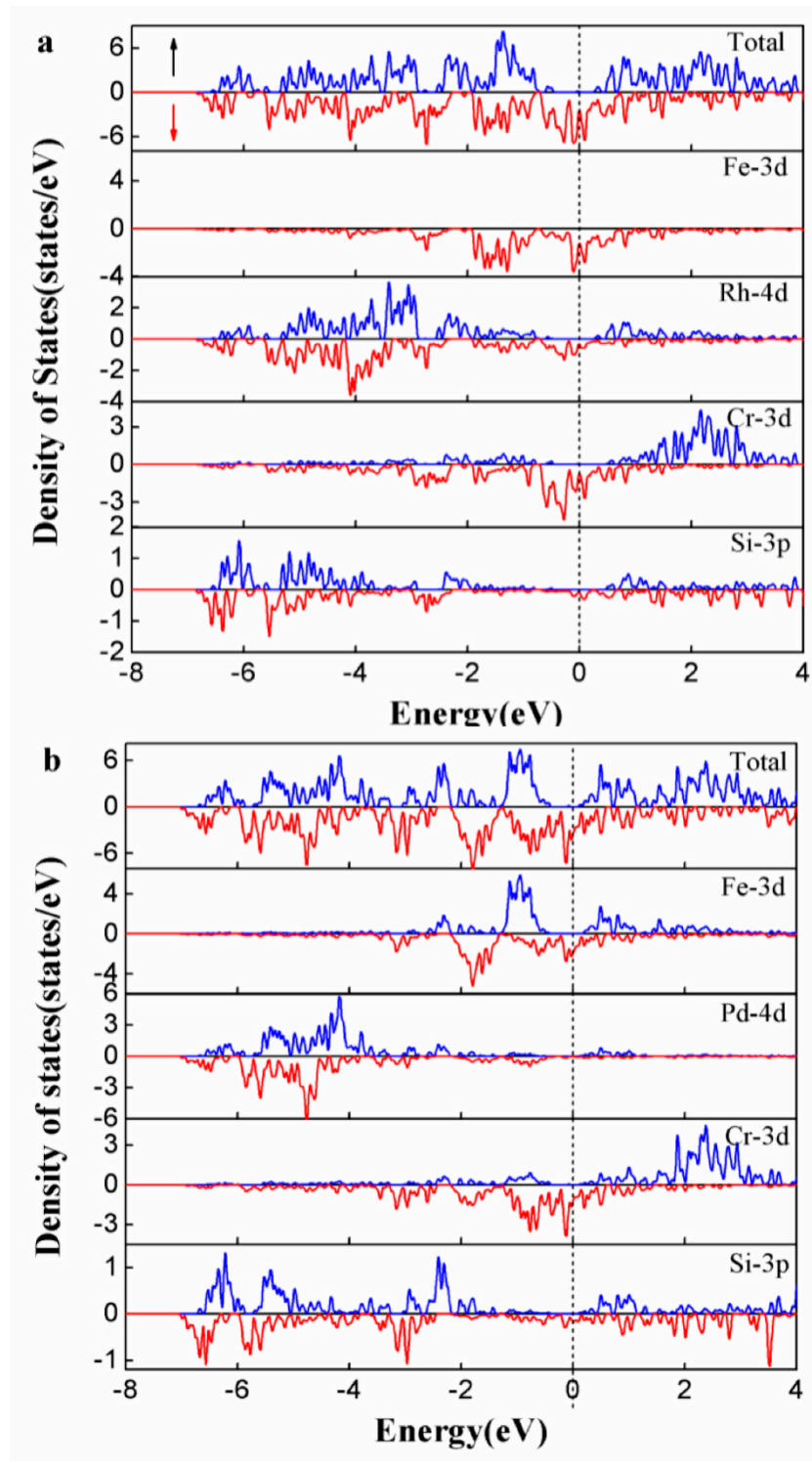
Figure 5. The total and partial density of states of (**a**) FeRhCrSi and (**b**) FePdCrSi at their equilibrium lattice constants.

The total and partial magnetic moments at the equilibrium lattice constant are listed in Table 2. The total magnetic moments (M_t) are integers for both FeRhCrSi and FePdCrSi compounds, which are 3 μB and 4 μB, respectively. The M_t follows the Slater–Pauling behavior, which can be expressed by $M_t = Z_t - 24$, where Z_t is the total number of valence electrons [35,36]. It can be found that the M_t is mainly from the Cr atom (3.10 μ_B and 3.44 μ_B for FeRhCrSi and FePdCrSi, respectively) and this is consistent with the above DOS discussion. Meanwhile, Fe, Rh, and Pd atoms have a small contribution to M_t.

Furthermore, due to the anti-parallel atomic magnetic moment among the Fe, Rh/Pd, and Cr atoms, both FeRhCrSi and FePdCrSi compounds exhibit a ferrimagnetic character.

3.3. Structural Stability

In order to test whether FeRhCrSi and FePdCrSi compounds can be synthesized and form a stable phase experimentally, the formation energy E_f and cohesive energy E_c were calculated in this work. The calculated values of the E_f and E_c are listed in Table 2. Taking FeRhCrSi as an example, the formation energy can be expressed by

$$E_f = E_{tot} - E_{Fe}^{bulk} - E_{Rh}^{bulk} - E_{Cr}^{bulk} - E_{Si}^{bulk} \tag{1}$$

Here, E_{tot} is the total energy of FeRhCrSi, E_{Fe}^{bulk}, E_{Rh}^{bulk}, E_{Cr}^{bulk} and E_{Si}^{bulk} are the total energies for each Fe, Rh, Cr, and Si atoms in their bulk states [37]. The bulk states that adopted in our calculation of Fe and Cr are body centered cubic(b.c.c) structure, Pd and Rh are face centered cubic(f.c.c) structure, and Si is diamond cubic(d.c) structure. The cohesive energy is expressed by

$$E_c = E_{tot} - E_{Fe}^{iso} - E_{Rh}^{iso} - E_{Cr}^{iso} - E_{Si}^{iso} \tag{2}$$

Here, E_{Fe}^{iso}, E_{Rh}^{iso}, E_{Cr}^{iso} and E_{Si}^{iso} refer to the energies of each isolated atom [37]. It can be found that formation energies for these alloys are both negative values, which are -3.12 eV for FeRhCrSi and -1.97 eV for FePdCrSi, indicating that these two alloys are stable and cannot be decomposed easily. Furthermore, these alloys have great negative cohesive energies, which are -20.41 eV for FeRhCrSi and -18.66 eV for FePdCrSi, implying that they have good chemical stability in practice and are likely to be synthesized in the experiment.

3.4. Mechanical Properties

In this section, we discuss the mechanical properties of the FeRhCrSi and FePdCrSi compounds. For cubic crystals, there are only three independent single-crystal elastic constants (C_{11}, C_{12} and C_{44}). According to these three elastic constants, other important elastic moduli can be calculated as the following formulas:

$$B = \frac{C_{11} + 2C_{12}}{3} \tag{3}$$

$$G_V = \frac{C_{11} - C_{12} + 3C_{44}}{5} \tag{4}$$

$$G_R = \frac{5C_{44}(C_{11} - C_{12})}{4C_{44} + 3(C_{11} - C_{12})} \tag{5}$$

$$G = \frac{G_V + G_R}{2} \tag{6}$$

$$E = \frac{9GB}{2B + G} \tag{7}$$

$$\delta = \frac{3B - 2G}{2(3B + G)} \tag{8}$$

$$A = \frac{2C_{44}}{C_{11} - C_{12}} \tag{9}$$

Here, B is the bulk modulus, G_V is the Voigt's shear modulus, G_R is the Reuss's shear modulus, G is the shear modulus, E is the Young's modulus, δ is the Possion's ratio, and A is the anisotropy factor.

Based on the above elastic moduli, we can examine the mechanical stability of these two EQHs FeRhCrSi and FePdCrSi according to the following Born and Huang [38] generalized stability criteria:

$$C_{44} > 0; \; \frac{C_{11} - C_{12}}{2}; \; B = \frac{C_{11} + C_{12}}{2} > 0; \; C_{12} < B < C_{11} \tag{10}$$

Table 3 lists all the calculated elastic constants for FeRhCrSi and FePdCrSi. From these calculated values, one can clearly see that our results for C_{11}, C_{12}, and C_{44} follow the generalized stability criteria. Thus, the FeRhCrSi and FePdCrSi compounds are mechanically stable.

Table 3. The calculated elastic constants C_{ij}, bulk modulus *B*, shear modulus *G*, Young's modulus *E* (GPa), Pugh's ratio B/G and anisotropy factor A for the EQH compounds FeRhCrSi and FePdCrSi.

Compounds	C_{11}	C_{12}	C_{44}	B	G	E	B/G	A
FeRhCrSi	294.7	112.9	106.6	173.5	100.0	251.7	1.74	1.17
FePdCrSi	179.4	121.5	75.1	140.8	45.9	124.2	3.07	2.59

Moreover, the Pugh's ratios *B/G* of FeRhCrSi and FePdCrSi compounds are 1.74 and 3.07, respectively. According to Pugh's criteria, the material tends to be ductile when the Pugh's ratio is larger than 1.75. Otherwise, the material tends to be brittle when the Pugh's ratio is less than 1.75. From Table 3, it can be seen that the Pugh's ratio of FeRhCrSi is less than 1.75, which indicates that FeRhCrSi is brittle. However, the Pugh's ratio of FePdCrSi is larger than 1.75, thus suggesting that FePdCrSi is ductile. Furthermore, the stiffness of the material can be characterized by Young's modulus E. The material will become stiffer when the value of E is higher. Thus, it can be said that the FeRhCrSi is stiffer than FePdCrSi.

3.5. Strain Effect on the Electronic and Magnetic Properties

In fact, the half-metallic character of HMs is very sensitive to external conditions (such as the temperature and train effect) in its application on spintronic devices. The change of the lattice constants can destroy the half-metallicity. Thus, the band structures and magnetism of FeRhCrSi and FePdCrSi under the strain effect (including hydrostatic strain and tetragonal deformation) have been calculated to test the thermal expansion and external strain effect on the half-metallicity of them. Here, the conduction band minimum (CBM) and the valence band maximum (VBM) as functions of the lattice constant and c/a ratio in the majority spin channel were calculated and plotted to describe the change of the half-metallic behavior of the FeRhCrSi and FePdCrSi compounds (as shown in Figures 6 and 7).
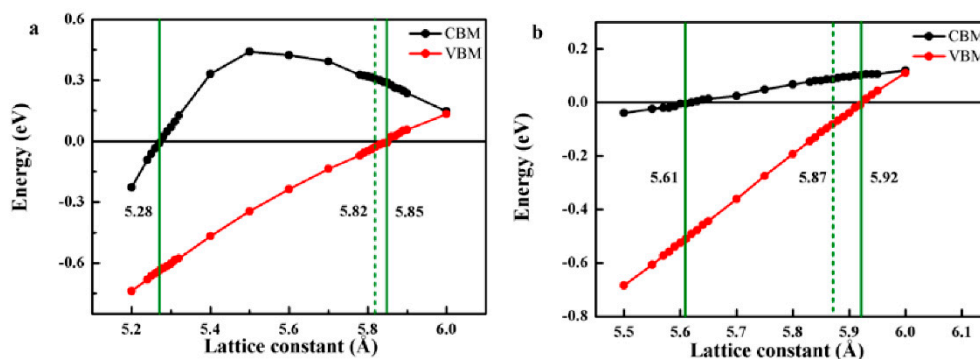

Figure 6. The conduction band minimum (CBM) and valence band maximum (VBM) in the majority spin channel as functions of lattice constants for (**a**) FeRhCrSi and (**b**) FePdCrSi compounds.
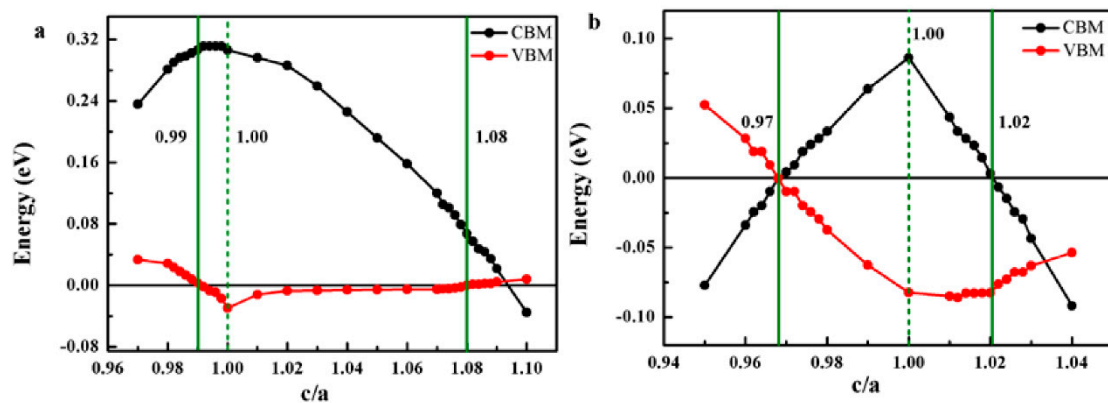
Figure 7. The CBM and VBM in the majority spin channel as functions of c/a ratios for (**a**) FeRhCrSi and (**b**) FePdCrSi compounds.

Figure 6 shows the CBM and VBM values under different hydrostatic strain for FeRhCrSi and FePdCrSi. From Figure 6, it can be obviously found that the half-metallicity of FeRhCrSi and FePdCrSi compounds can be kept in wide lattice constants that range from 5.28 Å–5.85 Å for FeRhCrSi and 5.61 Å–5.92 Å for FePdCrSi, respectively. This indicates that these two EQHs can keep their half-metallic properties in the lattice distortion range of −9.3% to 0.5% and −4.4% to 1% (relative to their equilibrium lattice constants). For FeRhCrSi and FePdCrSi compounds, it can be clearly seen that its half-metallic property is very robust to the lattice constant compression. Their half-metallicity cannot be destroyed until the lattice constant is compressed to 5.28 Å (by −9.3%) for FeRhCrSi and 5.61 Å (by −4.4%) for FePdCrSi, their conduction bands have an overlapping with the Fermi level at 5.28 Å and 5.61 Å. However, the half-metallicity of FeRhCrSi is relatively sensitive to the lattice constant expansion and their half-metallic properties will be destroyed when their lattice constants are expanded by about 0.5% and 1% for FeRhCrSi and FePdCrSi compounds, respectively.

Figure 7a,b show the VBM and CBM values under different c/a ratios in the range of 0.96–1.10 and 0.95–1.04 for FeRhCrSi and FePdCrSi, respectively. In this case, the cubic unit cells are compressed or stretched into a tetragonal one and the volumes of them are kept unchanged. As seen in Figure 7, it seems that their half-metallic properties are also robust to the tetrogonal deformation of lattice constants for FeRhCrSi and FePdCrSi compounds. In detail, FeRhCrSi and FePdCrSi compounds can keep their half-metallic properties when the c/a ratios change from 0.99 to 1.08 and 0.97 to 1.02, respectively. As the c/a ratios of FeRhCrSi and FePdCrSi decreases or increases from 1.0, their CBM value decrease and the value of VBM increases. Finally, this leads to the reduction or disappearance of their half-metallic band gaps. In order to further observe the change of the half-metallic bang gap with the tetragonal distortion, several majority-spin band structures around Fermi level at different c/a ratios for FeRhCrSi compound have been shown in Figure 8. From Figure 8, it can be clearly seen that the half-metallic band gap of FeRhCrSi decreases with tetragonal distortion and disappears at c/a = 0.97 and c/a = 1.02.

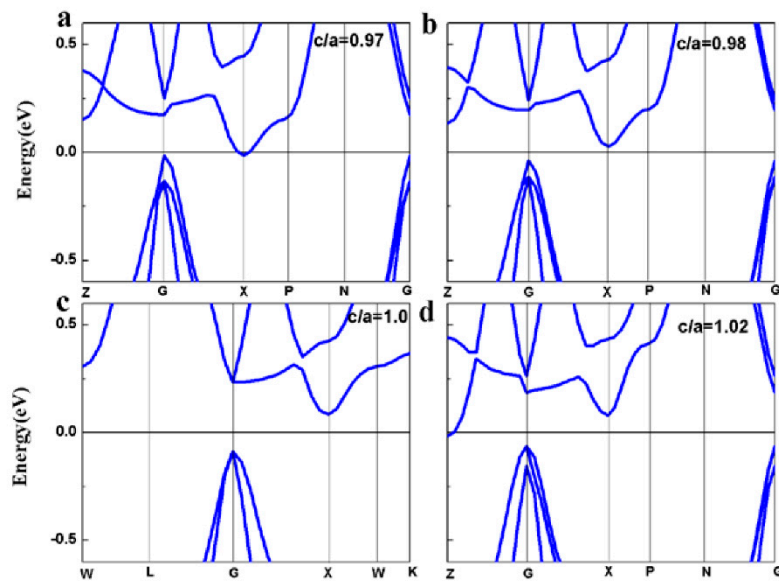**Figure 8.** The majority spin band structures around Fermi level at different c/a ratios for FePdCrSi compound (**a**) c/a = 0.97, (**b**) c/a = 0.98, (**c**) c/a = 1.0 and (**d**) c/a = 1.02.

In the next section, we will give a detailed discussion about the effect of the hydrostatic strain and tetragonal deformation on the magnetism of FeRhCrSi and FePdCrSi compounds. In Figures 9 and 10, the curves of the total and partial magnetic moments as functions of lattice constants and c/a ratios for FeRhCrSi and FePdCrSi are given. Clearly, one can observe that the total and partial magnetic moments of FeRhCrSi and FePdCrSi present quite a similar behavior with the change of the lattice constants and c/a ratios. From Figure 9, one can clearly observe that the total magnetic moments of both the FeRhCrSi and FePdCrSi compounds are always fixed into an integer value of 3 μ_B and 4 μ_B in the whole variational range. The atomic moments of the Fe and Cr atoms are very sensitive to the hydrostatic strain. The atomic moment of the Fe atom decreases with the increasing of the lattice constant. Whereas, the atomic moment of the Cr atom shows a growing trend with the increase of the lattice constant. Thus, the total magnetic moments of FeRhCrSi and FePdCrSi compounds can keep a fixed value in the whole variational range of the lattice constant. In Figure 10, one can observe that both the total and atomic magnetic moments of FeRhCrSi and FePdCrSi almost maintain an invariant constant with the variation of c/a ratios. This indicates that the magnetic properties of the FeRhCrSi and FePdCrSi are also not sensitive to the tetraganal deformation.
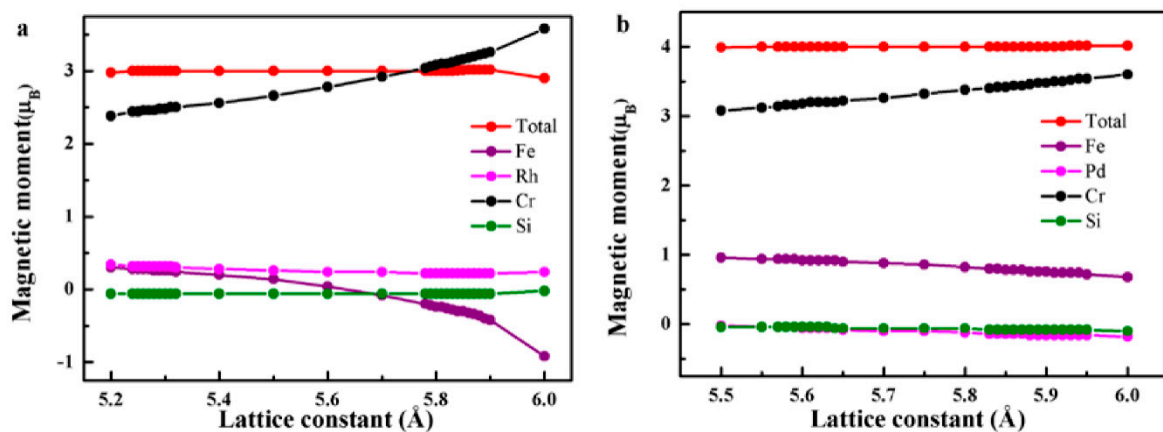

Figure 9. The total and partial magnetic moments as functions of lattice constants for (**a**) FeRhCrSi and (**b**) FePdCrSi.
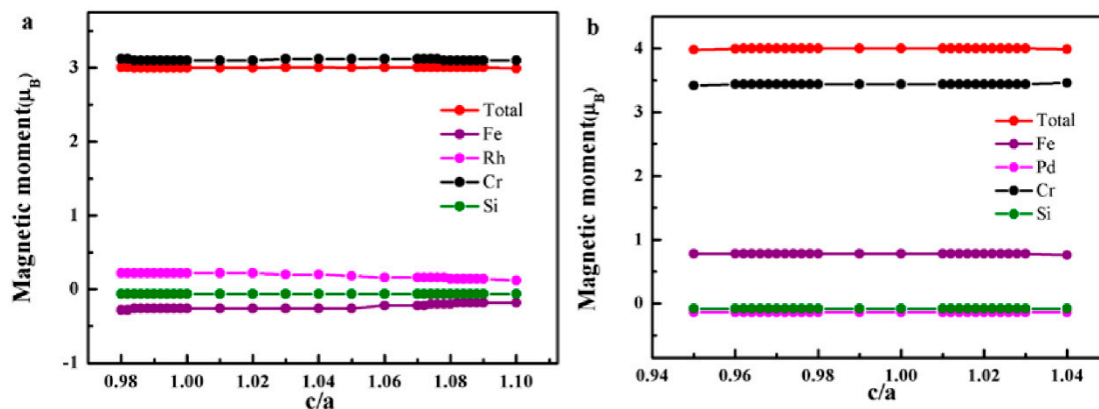
Figure 10. The total and partial magnetic moments as functions of c/a ratios for (**a**) FeRhCrSi and (**b**) FePdCrSi.

4. Conclusions

In summary, we have calculated the electronic, magnetic, half-metallic, structural stability and the mechanical properties of the new designed EQH compounds FeRhCrSi and FePdCrSi by using the first-principles method. The conclusions are listed as below:

(1)   FeRhCrSi and FePdCrSi compounds are two new ferrimagnetic HMs with a wide half-metallic band gap of 0.336 eV and 0.177 eV, respectively.

(2)   The half-metallicity of the FeRhCrSi and FePdCrSi compounds are very robust to the hydrostatic strain or tetragonal distortion. Especially for FeRhCrSi, the half-metallicity can be kept in a wide lattice constant range (5.28 Å–5.85 Å) under hydrostatic strain and a c/a ratios range (0.98–1.08) under tetragonal distortion, respectively.

(3)   The total magnetic moment of FeRhCrSi and FePdCrSi compounds are 3 μ_B and 4 μ_B, respectively, which obey the Slater–Pauling rule: $M_t = Z_t$-24. The main contributor of the total magnetic moments are both Cr atom for FeRhCrSi and FePdCrSi.

(4)   The large negative values of the calculated formation energy and cohesion energy show the direct evidence of the chemical and thermal stability for FeRhCrSi and FePdCrSi compounds. This indicates that they are likely to be synthesized in the experiment.

(5)   The elastic constants and the various moduli indicate the mechanical stability of FeRhCrSi and FePdCrSi compounds.

Author Contributions: L.Y. Wang designed the project. L.F. Feng and J.N. Ma performed the calculations and prepared the manuscript. All authors analyzed the data and discussed the results.

Conflicts of Interest: The authors declare no conflicts of interest.

References

1.   De Groot, R.A.; Mueller, F.M.; van Engen, P.G.; Buschow, K.H.J. New class of materials: half-metallic ferromagnets. *Phys. Rev. Lett.* **1983**, *50*, 2024. [CrossRef]

2.   Wang, X.; Cheng, Z.; Jin, Y.; Wu, Y.; Dai, X.; Liu, G. Magneto-electronic properties and tetragonal deformation of rare-earth-element-based quaternary Heusler half-metals: A first-principles prediction. *J. Alloys Compd.* **2018**, *734*, 329–341. [CrossRef]

3.   Sun, Q.; Kioussis, N. Prediction of manganese trihalides as two-dimensional Dirac half-metals. *Phys. Rev. B* **2018**, *97*, 094408. [CrossRef]

4.   Davatolhagh, S.; Dehghan, A. Dirac-like half-metallicity of $d^0 - d$ half-Heusler alloys. *Phys. C Supercond. Appl.* **2018**, *552*, 53–56. [CrossRef]

5.	Han, Y.; Wang, X. First-Principles Investigation of Half-Metallic Ferromagnetism of a New 1:1:1:1 Type Quaternary Heusler Compound YRhTiSi. *J. Supercond. Novel Magn.* **2018**. [CrossRef]

6.	Zhang, L.; Wang, X.T.; Rozale, H.; Gao, Y.C.; Wang, L.Y.; Chen, X.B. Electronic structures, magnetic properties and half-metallicity in Heusler alloys Zr_2IrZ (Zá = áAl, Ga, In). *Curr. Appl. Phys.* **2015**, *15*, 1117–1123. [CrossRef]

7.	Yu, W.; Zhu, Z.; Niu, C.Y.; Li, C.; Cho, J.H.; Jia, Y. Dilute Magnetic Semiconductor and Half-Metal Behaviors in 3 d Transition-Metal Doped Black and Blue Phosphorenes: A First-Principles Study. Nanoscale research letters. *Nanoscale Res. Lett.* **2016**, *11*, 77. [CrossRef] [PubMed]

8.	Galanakis, I.; Mavropoulos, P. Zinc-blende compounds of transition elements with N, P, As, Sb, S, Se, and Te as half-metallic systems. *Phys. Rev. B* **2003**, *67*, 104417. [CrossRef]

9.	Wurmehl, S.; Fecher, G.H.; Kandpal, H.C.; Ksenofontov, V.; Felser, C.; Lin, H.J. Investigation of Co 2 Fe Si: The Heusler compound with highest Curie temperature and magnetic moment. *Appl. Phys. Lett.* **2005**, *88*, 032503. [CrossRef]

10.	Kanomata, T.; Kyuji, S.; Nashima, O.; Ono, F.; Kaneko, T.; Endo, S. The Curie temperature in Heusler alloys Ni_2MnZ (Z = Ga, Sn and Sb) under high pressure. *J. Alloys Compd.* **2012**, *518*, 19–21. [CrossRef]

11.	Campbell, C.C.M. Hyperfine field systematics in Heusler alloys. *J. Phys. F: Met. Phys.* **1975**, *5*, 1931. [CrossRef]

12.	Peng, H.; Perdew, J.P. Rehabilitation of the Perdew-Burke-Ernzerhof generalized gradient approximation for layered materials. *Phys. Rev. B* **2017**, *95*, 081105. [CrossRef]

13.	Wang, R.; Zhao, Y.; Li, Z.; Chen, H.; Tao, X.; Ouyang, Y. The effect of Al content on the structural, mechanical, and thermal properties of B_2-FeAl and $D0_3$-Fe_3Al from atomistic study. *Mater. Res. Express* **2018**, *5*, 026512. [CrossRef]

14.	Jamer, M.E.; Wang, Y.J.; Stephen, G.M.; McDonald, I.J.; Grutter, A.J.; Sterbinsky, G.E.; Arena, D.A.; Borchers, J.A.; Kirby, B.J.; Lewis, L.H.; et al. Compensated Ferrimagnetism in the Zero-Moment Heusler Alloy Mn 3 Al. *Phys. Rev. Appl.* **2017**, *7*, 064036. [CrossRef]

15.	Helmholdt, R.B.; de Groot, R.A.; Mueller, F.M.; van Engen, P.G.; Buschow, K.H.J. Magnetic and crystallographic properties of several C1b type Heusler compounds. *J. Magn. Magn. Mater.* **1984**, *43*, 249–255. [CrossRef]

16.	Bainsla, L.; Suresh, K.G. Equiatomic quaternary Heusler alloys: A material perspective for spintronic applications. *Appl. Phys. Rev.* **2016**, *3*, 031101. [CrossRef]

17.	Dai, X.; Liu, G.; Fecher, G.H.; Felser, C.; Li, Y.; Liu, H. New quarternary half metallic material CoFeMnSi. *J. Appl. Phys.* **2009**, *105*, 07E901. [CrossRef]

18.	Klaer, P.; Balke, B.; Alijani, V.; Winterlik, J.; Fecher, G.H.; Felser, C.; Elmers, H.J. Element-specific magnetic moments and spin-resolved density of states in CoFeMn Z (Z = Al, Ga; Si, Ge). *Phys. Rev. B* **2011**, *84*, 144413. [CrossRef]

19.	Alijani, V.; Ouardi, S.; Fecher, G.H.; Winterlik, J.; Naghavi, S.S.; Kozina, X.; Stryganyuk, G.; Felser, C.; Ikenaga, E.; Yamashita, Y.; et al. Electronic, structural, and magnetic properties of the half-metallic ferromagnetic quaternary Heusler compounds CoFeMn Z (Z = Al, Ga, Si, Ge). *Phys. Rev. B* **2011**, *84*, 224416. [CrossRef]

20.	Alijani, V.; Winterlik, J.; Fecher, G.H.; Naghavi, S.S.; Felser, C. Quaternary half-metallic Heusler ferromagnets for spintronics applications. *Phys. Rev. B* **2011**, *83*, 184428. [CrossRef]

21.	Gao, G.Y.; Hu, L.; Yao, K.L.; Luo, B.; Liu, N. Large half-metallic gaps in the quaternary Heusler alloys CoFeCrZ (Z = Al, Si, Ga, Ge): A first-principles study. *J. Alloys Compd.* **2013**, *551*, 539–543. [CrossRef]

22.	Karimian, N.; Ahmadian, F. Electronic structure and half-metallicity of new quaternary Heusler alloys NiFeTiZ (Z = Si, P, Ge, and As). *Solid State Commun.* **2015**, *223*, 60–66. [CrossRef]

23.	Berri, S.; Ibrir, M.; Maouche, D.; Attallah, M. Robust half-metallic ferromagnet of quaternary Heusler compounds ZrCoTiZ (Z = Si, Ge, Ga and Al). *Comput. Condens. Matter* **2014**, *1*, 26–31. [CrossRef]

24.	Wang, X.T.; Cheng, Z.X.; Guo, R.K.; Wang, J.L.; Rozale, H.; Wang, L.Y.; Yu, Z.Y.; Liu, G.D. First-principles study of new quaternary Heusler compounds without 3d transition metal elements: ZrRhHfZ (Z= Al, Ga, In). *Mater. Chem. Phys.* **2017**, *193*, 99–108. [CrossRef]

25. Wang, X.T.; Khachai, H.; Khenata, R.; Yuan, H.K.; Wang, L.Y.; Wang, W.H.; Bouhemadou, A.; Hao, L.Y.; Dai, X.F.; Guo, R.K.; et al. Structural, electronic, magnetic, half-metallic, mechanical, and thermodynamic properties of the quaternary Heusler compound FeCrRuSi: A first-principles study. *Sci. Rep.* **2017**. [CrossRef] [PubMed]

26. Guo, R.; Liu, G.; Wang, X.; Rozale, H.; Wang, L.; Khenata, R.; Wu, Z.; Dai, X. First-principles study on quaternary Heusler compounds ZrFeVZ (Z = Al, Ga, In) with large spin-flip gap. *RSC Adv.* **2016**, *6*, 109394–109400. [CrossRef]

27. Segall, M.D.; Lindan, P.J.D.; Probert, M.J.; Pickard, C.J.; Hasnip, P.J. First-principles simulation: ideas, illustrations and the CASTEP code. *J. Phys. Condens. Matter* **2002**, *14*, 2717. [CrossRef]

28. Clark, S.J.; Segall, M.D.; Pickard, C.J.; Hasnip, P.J.; Probert, M.I.J.; Refson, K.; Payne, M.C. First principles methods using CASTEP. *Zeitschrift für Kristallographie-Cryst. Mater.* **2005**, *220*, 567–570. [CrossRef]

29. Cheeseman, J.R.; Frisch, M.J.; Devlin, F.J.; Stephens, P.J. Hartree-Fock and density functional theory ab initio calculation of optical rotation using GIAOs: Basis set dependence. *J. Phys. Chem. A* **2000**, *104*, 1039. [CrossRef]

30. Perdew, J.P.; Chevary, J.A.; Vosko, S.H.; Jackson, K.A.; Pederson, M.R.; Singh, D.J.; Fiolhais, C. Atoms, molecules, solids, and surfaces: Applications of the generalized gradient approximation for exchange and correlation. *Phys. Rev. B* **1992**, *46*, 6671. [CrossRef]

31. Steinmann, S.N.; Csonka, G.; Corminboeuf, C. Unified Inter- and Intramolecular Dispersion Correction Formula for Generalized Gradient Approximation Density Functional Theory. *J. Chem. Theory Comput.* **2009**, *5*, 2950. [CrossRef] [PubMed]

32. Umari, P.; Pasquarello, A. Polarizability and dielectric constant in density-functional supercell calculations with discrete k-point samplings. *Phys. Rev. B* **2003**, *68*, 085114. [CrossRef]

33. Rath, J.; Freeman, A.J. Generalized magnetic susceptibilities in metals: Application of the analytic tetrahedron linear energy method to Sc. *Phys. Rev. B* **1975**, *11*, 2109. [CrossRef]

34. Galanakis, I.; Dederichs, P.H.; Papanikolaou, N. Slater-Pauling behavior and origin of the half-metallicity of the full-Heusler alloys. *Phys. Rev. B* **2002**, *66*, 174429. [CrossRef]

35. Galanakis, I. Slater-Pauling Behavior in Half-Metallic Magnets. *J. Surf. Interface. Mater.* **2014**, *2*, 74–78. [CrossRef]

36. Fecher, G.H.; Kandpal, H.C.; Wurmehl, S.; Felser, C.; Schönhense, G. Slater-Pauling rule and Curie temperature of Co2Co2-based Heusler compounds. *J. Appl. Phys.* **2006**, *99*, 08J106. [CrossRef]

37. Srivastava, G.P.; Weaire, D. The theory of the cohesive energies of solids. *Adv. Phys.* **1987**, *36*, 463. [CrossRef]

38. Huang, K.; Born, M. Clarendon. In *Dynamical Theory of Crystal Lattices*; Clarendon Press: Oxford, UK, 1954; p. 420.